

Deep Joint Source Channel Coding for Secure End-to-End Image Transmission

Mehdi Letafati*, *Student Member, IEEE*, Seyyed Amirhossein Ameli Kalkhoran*, Ecnaz Erdemir, *Student Member, IEEE*, Babak Hossein Khalaj, *Senior Member, IEEE*, Hamid Behroozi, *Member, IEEE*, and Deniz Gündüz, *Fellow, IEEE*

Abstract—Deep neural network (DNN)-based joint source and channel coding is proposed for end-to-end secure image transmission against multiple eavesdroppers. Both scenarios of colluding and non-colluding eavesdroppers are considered. Instead of idealistic assumptions of perfectly known and i.i.d. source and channel distributions, the proposed scheme assumes unknown source and channel statistics. The goal is to transmit images with minimum distortion, while simultaneously preventing eavesdroppers from inferring private attributes of images. Simultaneously generalizing the ideas of *privacy funnel* and *wiretap coding*, a multi-objective optimization framework is expressed that characterizes the trade-off between image reconstruction quality and information leakage to eavesdroppers, taking into account the structural similarity index (SSIM) for improving the perceptual quality of image reconstruction. Extensive experiments over CIFAR-10 and CelebFaces Attributes (CelebA) datasets, together with *ablation studies* are provided to highlight the performance gain in terms of SSIM, adversarial accuracy, and cross-entropy metric compared with benchmarks. Experiments show that the proposed scheme restrains the adversarially-trained eavesdroppers from intercepting privatized data for both cases of eavesdropping a common secret, as well as the case in which eavesdroppers are interested in different secrets. Furthermore, useful insights on the *privacy-utility trade-off* are also provided.

Index Terms—Deep-JSCC, secure image transmission, end-to-end learning, privacy-utility trade-off, adversarial neural networks, deep learning.

I. INTRODUCTION

THE sixth generation (6G) of wireless networks is envisioned to realize *connected intelligence*, supporting an overabundance of disruptive technologies such as Internet-of-vehicles for autonomous driving [2], and haptic communications for extended reality (XR) and metaverse [3]. Recently, intelligent *multimedia transmission* is receiving much attention due to its various applications in XR, metaverse, and surveillance systems [4]. In this regard, if the transmission of source images is not properly secured, the performance of such services are no longer reliable.

Although different radio protocols have been proposed for the security of core network, the wireless edge of 6G networks

seem to face ever-increasing security threats, like man-in-the-middle attacks [5]–[7], spoofing [8], and eavesdropping [9], [10]. Fundamentally, this stems from the intrinsic open nature of the wireless medium, which makes transmitted signals susceptible to security and privacy risks. In this regard, deep neural network (DNN)-based approaches have shown to be capable of propelling the performance of wireless systems such that context-aware security can be achieved [11]–[13].

A. Motivation & Background

The communication of images from a source node, Alice, to a legitimate node, Bob, is a joint source channel coding (JSCC) problem. DNN-aided JSCC design, known as Deep-JSCC, has received significant attention in the recent years thanks to their superior performance, particularly their lack of reliance on accurate channel state information [14], [15]. In JSCC, unlike in separable source and channel coding, the transmitted channel codeword is correlated with the underlying source signal. While this benefits the legitimate encoder by providing robustness against channel noise, it also creates additional vulnerability in terms of leakage to eavesdroppers. Also note that classical encryption methods are not applicable here as they would destroy the correlation between the source and the channel input. The DNN-based design of JSCC is particularly attractive for the design of secure content delivery schemes, since they can learn the security sensitivity of different parts of the contents, and adopt their transmission strategy accordingly. Inspired by [16] and [17], this paper studies a generalization of the Deep-JSCC approach for secure end-to-end image transmission against multiple eavesdroppers, with both colluding and non-colluding eavesdropping strategies, and over AWGN as well as fading channels.

B. Prior Arts

In the context of secure end-to-end (E2E) communications, autoencoders were proposed in [18]–[20] for communication over AWGN wiretap channel. Feedforward neural networks composed of linear layers were employed as the encoder-decoder pair, and a weighted sum of block error rate and approximated information leakage was used as the loss function. The input data to the autoencoder was combined with additional non-informative random bits to confuse Eve, while such redundant bits can negatively affect the data rate. However, these works only focused on learning secure *channel coding* via DNNs rather than taking the source and channel coding jointly into account, i.e., undifferentiated with respect to the *content* of the message being delivered.

* Equal contribution.

Some preliminary results of this work were presented, in part, at IEEE Global Communications Conference, Kuala Lumpur, Malaysia, Dec. 2023 [1].

M. Letafati was with the EE Department of Sharif University of Technology, Tehran, 1365-11155, Iran (e-mail: mletafati@ee.sharif.edu), at the time of writing this paper. A. Ameli was with the CE Department of Sharif University of Technology, Tehran, Iran (e-mail: ameli@ce.sharif.edu), at the time of writing this paper. E. Erdemir was with the Department of Electrical and Electronic Engineering, Imperial College London, London SW7 2AZ, U.K. at the time of writing this paper. B. H. Khalaj, and H. Behroozi are with the EE Department of Sharif University of Technology, Tehran, Iran (e-mails: khalaj@sharif.edu, behroozi@sharif.edu). D. Gündüz is with the Department of Electrical and Electronic Engineering, Imperial College London, London SW7 2AZ, U.K. (e-mail: d.gunduz@imperial.ac.uk).

In the context of DNN-based secure wireless image transmission, [21] proposes cryptography-based approaches (public key cryptography) for secure transmission against one eavesdropper. It incorporates deep-JSCC scheme with encryption coding, proposing deep joint source-channel and encryption coding. The authors in [22] propose an image “protection” scheme with two additional DNN modules (so-called protection and de-protection), parameterized via U-Net added to the Deep-JSCC pipeline. The authors are mainly concerned about “application layer” digital content protection, and they do not take into account the privacy information leakage to eavesdroppers over wireless links. In [23], secure image transmission with Deep-JSCC as the neural model backbone for E2E communication is studied considering only the effect of one eavesdropper. This letter assumes the eavesdropper has access to a similar DNN model as of the legitimate nodes, and aims to reconstruct images. To combat the image reconstruction at the eavesdropper, the loss function for training the Deep-JSCC pipeline is simply modified by incorporating the mean squared error (MSE) between the source images and eavesdropper’s reconstruction, which is called “SecureMSE.” To apply SecureMSE for model training, it requires the statistical characteristics of the eavesdropping channel to be known by legitimate parties, which seems not to be feasible in practice, especially in the context of “totally passive” eavesdroppers. Recently, a preprint [24] studies the security of wireless image transmission against multiple eavesdroppers. However, the authors approach security from a totally different perspective than us, i.e., signal steganography. They propose two additional neural modules to be added to the encoder/decoder, calling it steganography modules. Finally, the security of Deep-JSCC-based wireless image transmission against active adversaries and backdoor attacks is studied in [25], which falls into the category of adversarial machine learning (AML) algorithms.

C. Our Contributions

We propose a Deep-JSCC-based solution for secure E2E wireless image transmission against *multiple eavesdroppers*. By employing Deep-JSCC pipeline, idealistic assumptions of perfectly known and i.i.d. source and channel distributions are dropped, and the proposed scheme assumes unknown source and channel statistics. Generalizing the ideas of privacy funnel and wiretap coding, the goal is to transmit images with minimum distortion, while simultaneously preventing eavesdroppers from inferring private image attributes, taking into account the perceptual quality metrics for image transmission and reconstruction. We consider both eavesdropping strategies, i.e., the colluding setup, in which the eavesdroppers cooperate with each other to extract sensitive/private part of images, and, the non-colluding setup, where the eavesdroppers act alone. We also study both cases of eavesdroppers being interested in a common secret, and the case in which every eavesdropper is interested in a different secret. Notably, previous works [16] and [17] only considered a single eavesdropper with a single-antenna transmitter and multiple parallel channels, respectively. In addition, both [16] and [17] are limited to

static channels. While we assume two well-established time-varying wireless channel models. That is, our proposed scheme is trained over complex-valued Rayleigh fading channels, and tested over Nakagami- m and AWGN channels in addition to Rayleigh-fading. Our proposed approach restrains adversarially-trained eavesdropping nodes from intercepting private information, in a way that they cannot correctly infer certain sensitive attributes. Moreover, (different from [18], [19]) no additional redundant bits are required to be added to the source image. Different from [22], [24], our scheme does not require any additional module to be added to the normal data pipeline of Deep-JSCC. Instead, we modify the loss function to come up with a secure and *privacy-aware* training and inference strategy for the communication entities, taking the information leakage and perceptual quality of images into account.

Our scheme relies on a *data-driven* approach, i.e., we do not consider any specific assumption on the underlying distribution of the data source or the sensitive/private part. Instead, we have access to datasets to facilitate the process of learning secure encoder-decoder pairs. To highlight the generalization of our proposed scheme, we evaluate our system using two different datasets of CIFAR-10¹ and CelebFaces Attributes (CelebA)². We demonstrate the performance gain of our approach, in terms of structural similarity index (SSIM), cross entropy (CE) metric, adversarial accuracy, and reconstruction quality through extensive experimental studies in various communication scenarios for both CIFAR-10 and CelebA datasets. Furthermore, we also conduct *ablation studies* to further study the effect of different hyperparameters of the implemented DNNs and the loss function on the E2E performance.

Finally, we would like to highlight the main differences between our paper and the prior work of [16]. 1) Our proposed scheme considers both scenarios of AWGN and fading channels, while [16] only considers an AWGN channel. 2) Our model is designed for secure transmission against multiple eavesdroppers, with different eavesdropping strategies, while [16] simply considers one Eve. 3) Our neural architecture differs from [16]. We do not simply employ “fully-convolutional” DNNs, but also utilize generalized normalization transformation (GDN) blocks, and their inverse counterpart (IGDN), [26] at the hidden layers. This has been shown to be able to provide significant improvements in capturing image statistics of natural images. We note that our performance improvements obtained over [16] are verified through different ablation studies in the simulation section. 4) Our model is trained based on a mixed loss function which not only considers the pixel-wise reconstruction (via the mean-squared-error), but also takes into account the *perceptual quality* of images through the SSIM metric. However, the prior work [16] only considers the pixel-wise peak signal-to-noise ratio (PSNR) metric. Unlike PSNR, the SSIM metric is a perception-based metric, which captures pixel inter-dependencies, and hence, the semantics of the source image.

¹<https://www.cs.toronto.edu/~kriz/cifar.html>

²<https://mmlab.ie.cuhk.edu.hk/projects/CelebA.html>

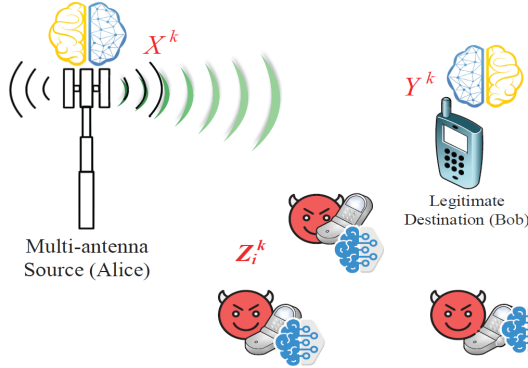


Fig. 1: Proposed learning-based system model for secure wireless image transmission against multiple eavesdroppers.

D. Paper Organization and Notations

The remainder of this paper is organized as follows. In Section II, our proposed system model together with the main assumptions and intuitions are provided. We also formulate our problem to characterize the funnel-like security framework. In Section III we propose our learning-based E2E approach to solve our problem in a data-driven manner. In Section IV, we investigate the performance of our scheme through extensive numerical experiments. We also compare our learning-based scheme with different benchmarks. Finally, Section V concludes our paper.

Notations: We denote the transpose, the conjugate transpose, and ℓ^2 norm of a vector by $(\cdot)^T$, $(\cdot)^\dagger$, and $\|\cdot\|$, respectively. Vectors are represented by bold lowercase letters. The zero and the identity matrices are shown by $\mathbf{0}$ and \mathbf{I} , respectively. $\mathcal{CN}(\mu, \sigma^2)$ and $\mathcal{G}(k, \theta)$ represent a complex random variable (RV) with mean μ and standard deviation σ , and gamma distribution with shape parameter k and scale parameter θ , respectively. The expected value and the probability density function (pdf) of RV X are denoted by $\mathbb{E}[X]$ and $p_X(x)$, respectively. The mutual information of RVs X and Y and the cross-entropy of two distributions p and q are shown, respectively, by $I(X; Y)$ and $H(p, q)$.

II. SYSTEM MODEL AND PROBLEM STATEMENT

A. Model Description

Consider the communication scenario demonstrated in Fig. 1, where a multi-antenna source node, Alice (\mathcal{A}), aims to transmit images $U^n \in \mathcal{U}^n$ to a destination node, Bob (\mathcal{B}), over k uses of the wireless channel, where \mathcal{U} denotes the alphabet of source images. According to the JSCC literature [14], we refer to the image dimension, n , as the source bandwidth. The channel dimension k characterizes the channel bandwidth. We usually have $k < n$, which reflects the concept of bandwidth compression (please see [14] and references therein for more details). The image transmission service should be kept secret from multiple eavesdroppers, which overhear the communication and are equipped with adversarial DNNs, aiming to extract private data regarding the source image. \mathcal{A} and \mathcal{B} employ DNNs and perform *secure Depp-JSCC* by leveraging the concept of autoencoders. Details of the proposed DNN architectures, together with the training strategies of legitimate

autoencoder and adversarial neural decoders are given in the next sections.

Alice aims to convey the source information U^n to Bob with minimum distortion, while preventing the information of sensitive part $S_i \in \mathcal{S}_i$, with a discrete alphabet \mathcal{S}_i , to be leaked to the i -th eavesdropper, $i = 1, \dots, M$, where M denotes the number of eavesdroppers. We note that the sensitive (private) parts are correlated with U^n with distribution $p_{U^n, S_1, S_2, \dots, S_M}$. Toward this end, Alice maps the source information U^n into a channel input codeword $X^k \in \mathcal{X}^k$ via implementing a potentially non-trivial function $f_A : \mathcal{U}^n \rightarrow \mathcal{X}^k$, where $X^k = f_A(U^n)$. Transmitted codeword is subject to an average power constraint, $\frac{1}{k} \mathbb{E}[(X^k)^* X^k] \leq P$. Channel outputs at Bob and the i 'th eavesdropper are denoted, respectively, by Y^k and Z_i^k , $i \in \{1, \dots, M\}$. Bob then applies a decoding function f_B to obtain $\hat{U}^n = f_B(Y^k)$. Meanwhile, each eavesdropper tries to extract the sensitive information S_i , that he is interested in, from his observations Z_i^k . We consider the trade-off between delivering images to Bob with the highest fidelity and controlling the information leakage to each adversary, which is theoretically measured by the mutual information metric $I(S_i; Z_i^k)$. In the case that all eavesdroppers are interested in the same secret we have $S_i = S, \forall i$.

Transmission of data-streams over the air experiences independent realizations of communication channels. Generally speaking, the channels impose random corruption on any transmitted symbol vector $\tau \in \mathbb{C}^k$, which we model through the transfer function $\eta(\tau)$. We consider both the AWGN and slow fading channels, where for the slow fading, we adopt two widely-used assumptions of Rayleigh fading and Nakagami- m channels. The transfer function of the Gaussian channel can be formulated by $\eta_\nu(\tau) = \tau + \nu$, where the vector $\nu \in \mathbb{C}^k$ is comprised of independent identically distributed (i.i.d.) samples from a circularly symmetric complex Gaussian distribution, i.e., $\nu \sim \mathcal{CN}(\mathbf{0}, \sigma^2 \mathbf{I}_k)$, where σ^2 is the average power of additive noise. For the fading scenario, the multiplicative effect of the communication channel is modeled by $\eta_h(z) = h\tau$, where $h \sim \mathcal{CN}(0, \delta_h^2)$ for the Rayleigh fading scenario, and $|h|^2 \sim \mathcal{G}(m, \delta_h^2/m)$ for the Nakagami- m scenario with $m > 1$. Here, δ_h represents the standard deviation (std) of the channel distribution, which reflects the large-scale effects of channel fading. The joint effect of channel fading and Gaussian noise can be treated by the composition of transfer functions as $\eta(\tau) = \eta_\nu(\eta_h(\tau)) = h\tau + \nu$.

Fundamentally, the trade-off between the minimum achievable distortion at the legitimate receiver and the minimum leakage to Eve is asymptotically characterized in [27] under the idealistic assumption of i.i.d. source and channels with known distributions. However, this result is not applicable to practical systems with finite block-lengths and unknown source and channel statistics. Hence, in our system model we consider a *data-driven* approach for the practical non-asymptotic regime. That is, we do not consider any underlying assumption on the distribution of the data source or the latent private variable. We remark that while we do assume a known channel model, we use this model to generate samples from conditional channel distribution. We could easily drop this assumption if we had data collected from a particular channel

with unknown statistics.

B. Problem Formulation

Inspired by the key idea of *privacy funnel* [28], we first formulate an optimization framework to characterize the trade-off between successful image recovery at Bob and the information leakage to the eavesdroppers, which we call *secrecy funnel*. The formulated funnel-like framework is then solved in a data-driven manner, utilizing Deep-JSCC architecture. That is, we implement DNNs, based on the concept of autoencoders, to learn the secure encoding-decoding functions, while restraining the adversarially-trained eavesdroppers from intercepting private information.

We aim to simultaneously minimize both the distortion $d(U^n, \hat{U}^n)$ at Bob and the information leakage, $I(S_i; Z_i^k)$, $i \in [M]$, about the secrets S_i , to adversaries. This corresponds to a multi-objective programming (MOP) that can be solved using the scalarization approach [29]. That is, we minimize a weighted sum of the multiple objectives with weights $w_i \in \mathbb{R}_{>0}$ as follows

$$\underset{p_{X^k|U^n}, f_B}{\text{minimize}} \quad \mathbb{E} \left[d(U^n, \hat{U}^n) \right] + \frac{1}{M} \sum_{i \in [M]} w_i I(S_i; Z_i^k). \quad (1)$$

Notably, w_i in (1) shapes our secrecy funnel for each private attribute, i.e., it adjusts the trade-off between the information leakages and the distortion at the legitimate receiver. To make the proposed MOP in (1) tractable, we further need to estimate the mutual information term in our problem. More specifically, it is still a major challenge to optimize DNNs, while having an objective function comprised of expressions about the mutual information between two (or more) data distributions. It is also challenging to directly estimate the mutual information metric from samples according to [16], [18], [19]. In other words, we need to find an appropriate ‘‘interpretation’’ for the characterized secrecy funnel in (1), in order to make the DNNs ‘‘understand’’ the secrecy framework and take proper actions during inference. To reach this goal, in the following we propose a secrecy criterion based on the cross-entropy (CE) metric, which is also interpretable for the training of the DNN models within the Deep-JSCC-based secure image transmission pipeline.

We first apply the variational approximation proposed in [30] for the mutual information metric and obtain

$$\underset{p_{X^k|U^n}, f_B}{\text{minimize}} \quad \mathbb{E} \left[d(U^n, \hat{U}^n) \right] + \frac{1}{M} \sum_{i \in [M]} w_i \max_{q_{S_i|Z_i^k}} \mathbb{E} \left[\log q_{S_i|Z_i^k}(s_i|z_i) \right], \quad (2)$$

where $q_{S_i|Z_i^k}(s_i|z_i)$ characterizes the i 'th adversary's likelihood estimation corresponding to the correct distribution of S_i , given the observation Z_i^k . The goal of this approximation is that we can further interpret the variational lower bound utilized in (2) as the sample-wise CE between the distribution over adversaries' predictions and the true distribution of sensitive attributes. More details are given in the next sections.

Invoking (2), one can infer that it can be viewed as a minimax game between Alice-Bob pair, and the set of adversaries. To elaborate, while adversarial nodes wish to maximize

their individual information leakage by choosing the posterior likelihood distributions $q_{S_i|Z_i^k}$, Alice and Bob should jointly determine the optimum encoding-decoding functions, f_A and f_B , to optimally shape the secrecy funnel that minimizes the weighted sum of the distortion and leakage. Nevertheless, we emphasize that we do not assume to have any knowledge about the underlying distribution of image source and the sensitive attributes, which is aligned with the real-world scenarios. Our scheme relies upon a *data-driven* approach, i.e., we leverage datasets to ‘‘learn’’ the optimized E2E secure encoding-decoding functionalities.

To solve the proposed MOP of (2) in a data-driven manner, we implement DNNs to parameterize the optimized secure encoding-decoding functionalities at Alice and Bob, while the adversaries also employ optimized adversarially-trained DNNs and try to infer the sensitive attribute of the transmitted image. Let Ω_A and Ω_B stand for the set of (trainable) parameters of the autoencoder pair at Alice and Bob, respectively. In addition, let $\Theta_{E,i}$ parameterize the adversarial network of the i 'th adversary. We can formulate the following loss function to be minimized.

$$\begin{aligned} \mathcal{L}(\Omega_A, \Omega_B, \Theta_{E,1}, \dots, \Theta_{E,M}) &= \mathbb{E} \left[d(U^n, f_{\Omega_B}(Y^k)) \right] \\ &+ \frac{1}{M} \sum_{i \in [M]} w_i \max_{\Theta_{E,i}} \mathbb{E} \left[\log q_{\Theta_{E,i}}(s_i|z_i) \right], \quad (3) \end{aligned}$$

where f_{Ω_A} and f_{Ω_B} represent the encoder and decoder functionality of Alice's DNN and Bob's DNN, respectively, for which we have $X^k = f_{\Omega_A}(U^n)$. Moreover, $q_{\Theta_{E,i}}(s_i|z_i)$ formulates the approximated adversarial likelihood about the correct value $S_i = s_i$, estimated at the DNN of the i 'th adversary with parameters $\Theta_{E,i}$ and based on the observation $Z_i^k = z_i$. We emphasize that similarly to [14]–[16], the legitimate and wiretap channels are treated as non-trainable layers. However, since the considered channels are differentiable, we incorporate them as part of our proposed E2E secure transmission scheme.

In the following, we leverage the novel concept utilized in generative adversarial networks (GANs) and iteratively train the DNNs based on the loss function proposed in (3). To elaborate, each joint training phase of the autoencoder pair (Ω_A, Ω_B) is followed by a training step for the adversaries' parameters ($\Theta_{E,1}, \Theta_{E,2}, \dots, \Theta_{E,M}$), where more details are given in the next section. In what follows, we also address context-aware interpretations for the distortion measure and the likelihood distribution of sensitive attributes, which leads us toward a machine learning-interpretable approach for E2E secure communication.

III. PROPOSED DEEP JSCC-BASED SOLUTION

Following the Deep-JSCC concept, we employ DNNs to directly map the pixel values to the complex-valued samples, which are sent over the air. Consider image input files with dimensions $n = H \times W \times C$, where H , W , and C stand for the image height, width, and the number of channels (3 for colored images and 1 for grayscale), respectively. Alice maps each realization of the source data U^n , denoted by $\mathbf{u} \in \mathbb{R}^n$, to a vector of channel input $\mathbf{x} \in \mathbb{C}^k$, which can be viewed as a

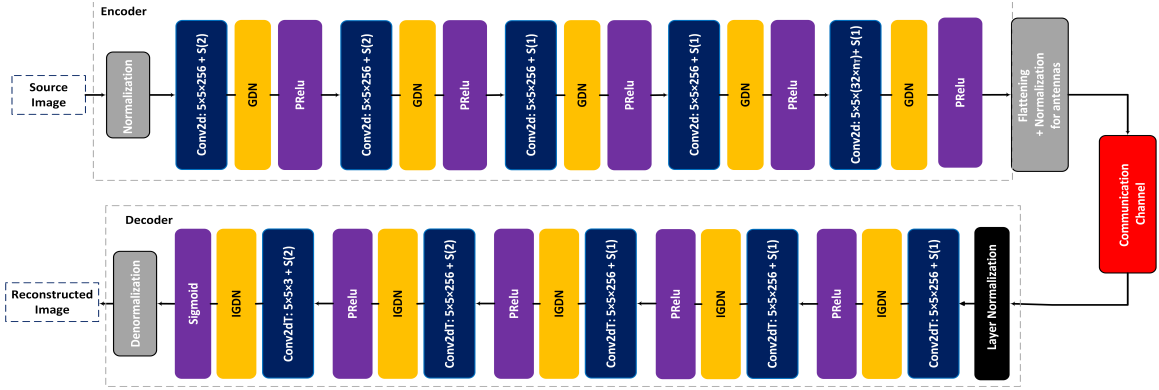


Fig. 2: Proposed deep neural networks at Alice (encoder) and Bob (decoder). The notation $w \times w \times f$ denotes a convolutional layer with f filters (channel outputs) of spatial extent w . The notation $w \times w \times (f \times n_T)$ at the last convolutional layer of encoder indicates that we require f filters for each of n_T antennas at the encoder output. Moreover, $s(\cdot)$ denotes the stride, which can be downsampling (at the encoder) or upsampling (at the decoder).

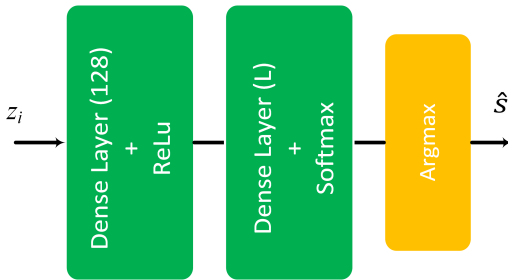


Fig. 3: Implemented DNN at each of the adversaries for extracting sensitive part of image files.

realization of X^k . x should be securely encoded at Alice and decoded by Bob to realize secure data communication against multiple adversarial DNNs, based on the objective introduced in (3). This is done via our proposed DNN-based solution, where the block diagram of the DNNs employed for the neural encoder and decoder components of legitimate parties is illustrated in Fig. 2. In addition, the DNN employed by each of the adversaries is demonstrated in Fig. 3. The structure of each DNN component is described next.³

A. Legitimate Neural Encoder-Decoder Pair:

At the legitimate encoder, we implement convolutional layers, followed by normalization invoked by the generalized normalization transformations (GDN) block [26], which is then followed by a parametric ReLU (PReLU) [31] activation function. At the output of the last PReLU layer, which consisting of $2k \times n_T$ elements, we employ a flattening layer for each of the antennas, to reshape the encoded tensor to a data-stream from the latent space, resulting in a data sequence of the form $\tilde{x}_i \in \mathbb{C}^k$ for each antenna $1 \leq i \leq n_T$. The encoded latent sequence is further normalized, such that the channel input $\mathbf{X} \triangleq [\mathbf{x}_1, \mathbf{x}_2, \dots, \mathbf{x}_{n_T}] \in \mathbb{C}^{k \times n_T}$ satisfies the average transmit power constraint P . Mathematically speaking, we have

$$\mathbf{x}_i = \sqrt{kP} \frac{\tilde{\mathbf{x}}_i}{\sqrt{\tilde{\mathbf{x}}_i^\dagger \tilde{\mathbf{x}}_i}}, \quad 1 \leq i \leq n_T. \quad (4)$$

Each column of the channel input data matrix \mathbf{X} is then distributed over each of n_T antennas to exploit the available degrees of freedom.

The joint source-channel coded output of Alice's DNN is sent over the communication channel, where the quality of the information-bearing sequence will be corrupted due to additive noise, fading, or other channel impairments. The channel distorted version $\mathbf{y} \in \mathbb{C}^k$ is observed by Bob, where \mathbf{y} is considered as a realization of Y^k , i.e., the output of the communication channel. Accordingly, \mathbf{y} is fed to Bob's DNN, which tries to recover the image by estimating $\hat{\mathbf{x}} \in \mathbb{R}^n$ from \mathbf{y} , resulting in an approximate reconstructed version of the original data. Specifically, the real and imaginary parts of the k (complex-valued) channel output samples form $2k$ real-valued elements, which are fed into the convolutional layers. Based on the encoding conducted by Alice, Bob's DNN inverts the operations implemented at Alice by passing the observed data-stream \mathbf{y} through a series of transposed convolutional layers followed by the inverse of GDN (IGDN) blocks and PReLU activation functions.

The intuition behind the proposed architecture for can be explained as follows. Convolutional layers are capable of extracting image features. After that the convolutional layers have extracted the features, the GDNs (which perform differentiable and invertible operations) conduct local divisive normalization, which has been shown to be effective in density modeling of data [26]. Moreover, the GDNs offer significant improvements in capturing image statistics through Gaussianizing the data of natural images. In the next step, the activation functions facilitate the learning process of non-linear mappings from the source image space to the latent space, i.e., the channel input, and vice versa. Finally, the hyperparameters of Bob's DNN mirror the corresponding functionalities performed by the encoder layers of Alice's DNN.

Remark 1: We remark that before running the proposed DNNs, the input images are normalized by the maximum pixel value, e.g. 255 in this paper, to produce values in the

³We state that the considered hyper-parameters for the legitimate DNNs, as demonstrated in Fig. 2, are selected based on comprehensive experiments and numerous trials, while the general architecture is inspired by [15].

range of $[0, 1]$. This operation will be inverted at the decoder (as demonstrated in Fig. 2) to reconstruct (de-normalized) pixel values within $[0, 255]$ range. The rationale behind this reformulation is that the dependence of DNNs on the maximum pixel values is relaxed, since the statistics of data are unknown at the decoder. This also facilitates the training process of our proposed DNNs [12]. Notably, the sigmoid activation function applied to the output of Bob's decoder is for producing normalized approximation (\hat{x}) for the original data in the range of $[0, 1]$ before de-normalizing.

Remark 2: Prior to performing DNN-based decoding operations, a layer normalization (LN) block [32] is implemented at Bob's DNN. The LN block is aimed to realize data normalization via taking into account all of the summed inputs to the Bob's DNN during *every single training or inference sample*. Notably, unlike batch normalization which considers the distribution of the summed input to a neuron over *mini-batches* of training set, LN performs the same computation at training and inference phases *per data sample*. It is also shown in [32] that compared with previous techniques, LN substantially reduces the training time.

B. Adversarial Neural Networks for Eavesdroppers

The structure of adversarial DNNs, which are parameterized by $\Theta_{E,i}, i \in [M]$, is presented in Fig. 3. According to the proposed system model in Section II-A, the adversaries utilize DNNs to facilitate the extraction of sensitive information S_i from their received signals. The sensitive information S_i can be assumed to be the class to which the images belong [16], [17]. For instance, the identity of patients within medical imaging in e-health applications, or the locations of critical infrastructures in a cyber-physical system. To extract sensitive information (e.g., privatized data) from images, each adversary employs the DNN architecture illustrated in Fig. 3 as a class predictor, which is comprised of a dense layer (fully-connected network with 128 neurons) with rectified linear unit (ReLU) activation function. The dense layer is concatenated by another dense layer with softmax activation, where the dimension of the output neurons, L , equals the cardinality of the secret $|S_i|$. The output of the softmax layer produces an adversarial likelihood estimation regarding the posterior distribution $q_{\Theta_{E,i}}(s_i|z_i)$ of sensitive attribute.⁴ Specifically, considering the output $z_i \in \mathbb{C}^k$ of the i 'th wiretap channel (a realization of Z_i^k) as the observation of the i 'th eavesdropper, it is fed to the adversarial DNN to obtain an approximated prediction $q_{\Theta_{E,i}}(s_i|z_i)$ regarding the sensitive attribute.

Invoking (3), each adversary tries to minimize its CE between the adversarially-estimated likelihood distribution and the ground-truth, which is represented by the one-hot encoded vector of S_i , denoted by $\varepsilon_{s_i} \in \{0, 1\}^L$. Notably, having lower CE values results in higher similarity between the posterior adversarial likelihood $q_{\Theta_{E,i}}(s_i|z_i)$ and the ground-truth ε_{s_i} , which increases the information leakage in terms of CE. Meanwhile, Alice and Bob jointly try to minimize the reconstruction distortion $d(\cdot, \cdot)$ and the information leakage to

adversarial DNNs measured by the negative CE metric $H(\cdot, \cdot)$. Exploiting the above-mentioned learning-based interpretation, our sample-wise secure framework can be reformulated as

$$\begin{aligned} \text{minimize } \mathcal{L}(\Omega_A, \Omega_B, \Theta_{E,1}, \Theta_{E,2}, \dots, \Theta_{E,M}) = \\ \mathbb{E}_{p(\mathbf{u}, \hat{\mathbf{u}})} [d(\mathbf{u}, f_{\Omega_B}(\mathbf{y}))] \\ + \frac{1}{M} \sum_{i \in [M]} w_i \max_{\Theta_{E,i}} (-H(q_{\Theta_{E,i}}(s_i|z_i), \varepsilon_{s_i})), \end{aligned} \quad (5)$$

where $\hat{\mathbf{u}} = f_{\Omega_B}(\mathbf{y})$, and $p(\mathbf{u}, \hat{\mathbf{u}})$ stands for the joint probability distribution of the original and the reconstructed image. Due to the fact that the true distribution of data $p(\mathbf{u})$ is often unknown, obtaining an analytical (closed-form) solution for (5) is not tractable [14]–[16], [19]. Thus, we estimate the expected distortion measure using samples \mathbf{u}_j of available datasets by computing $\mathbb{E}_{p(\mathbf{u}, \hat{\mathbf{u}})} [d(\mathbf{u}, f_{\Omega_B}(\mathbf{y}))] \approx \frac{1}{N_T} \sum_{j=1}^{N_T} d(\mathbf{u}_j, \hat{\mathbf{u}}_j)$, where N_T stands for the number of training samples. We note that, in this framework, we are assuming that we know the sensitive attribute each eavesdropper is interested in and their channel models, both of which are common assumptions in the privacy [16], [17], [28] and wiretap channel [19], [27] literature.

To achieve the proposed objective for our communication system in (5), both the legitimate and the adversarial DNNs should learn to optimize their network parameters. After the DNNs are trained, Alice, Bob and adversaries can run their DNNs online, every time a new image is required to be securely delivered.

C. Training Procedure

In order to train our learning-based approach based on the objective function proposed in (5), we follow an iterative procedure. Inspired by the key idea of GANs, each joint training phase of the autoencoder pair (Ω_A, Ω_B) is followed by a training step for the adversarial networks ($\Theta_{E,1}, \Theta_{E,2}, \dots, \Theta_{E,M}$). Intuitively, we are faced with a minimax game, i.e., the competition between legitimate autoencoder and the adversarial DNNs. Therefore, the following strategy is run through our proposed E2E system.

- (i) The pair of Alice and Bob try to jointly minimize their loss function,

$$\mathcal{L}_{AB} = \frac{1}{N_T} \sum_{j=1}^{N_T} \left(d(\mathbf{u}_j, \hat{\mathbf{u}}_j) - \frac{1}{M} \sum_{i \in [M]} w_i H(q_{\Theta_{E,i}}(s_i^{(j)}|z_i^{(j)}), \varepsilon_{s_i^{(j)}}) \right) \quad (6)$$

To reinforce system's security against adversaries, we take one further step within the training process of legitimate nodes. We perform *adversarial likelihood compensation* (ALC), which has been shown to be more effective in confusing an adversary than the data-dependent one-hot encoding approach [16]. The main idea behind the ALC is that we want to make the estimated likelihood of adversaries imitate a uniform distribution $\bar{p}_L = [\frac{1}{L}, \dots, \frac{1}{L}]^T$. By doing so, Alice and Bob try to jointly maximize the uncertainty of adversarial predictions by maximizing the similarity (i.e., minimizing the

⁴An argmax layer is added over the obtained distribution to take a guess about the predicted secret class \hat{s} . This also helps assess the performance of adversaries via measuring their accuracy as the fraction of correct guesses.

CE) between the adversarial likelihood and the uniform distribution \bar{p}_L , instead of minimizing the likelihood corresponding to the correct prediction ε_{s_i} . Hence, a revised objective function for Alice-Bob pair is formulated as

$$\mathcal{L}_{AB}^{\text{ALC}} = \frac{1}{N_{\mathcal{T}}} \sum_{j=1}^{N_{\mathcal{T}}} \left(d(\mathbf{u}_j, \hat{\mathbf{u}}_j) + \frac{1}{M} \sum_{i \in [M]} w_i H(q_{\Theta_{E,i}}(s_i^{(j)} | z_i^{(j)}), \bar{p}_L) \right) \quad (7)$$

- (ii) Each step of the joint training for \mathcal{A} -to- \mathcal{B} autoencoder ($\Omega_{\mathcal{A}}, \Omega_{\mathcal{B}}$) is followed by a training step for the adversarial DNNs. Eavesdroppers seek to minimize the CE between their estimated likelihood $q_{\Theta_{E,i}}(s_i | z_i)$ and the one-hot encoded vector ε_{s_i} corresponding to S_i . That is, we have the following loss function for training the adversarial networks.

$$\mathcal{L}_E = \frac{1}{N_{\mathcal{T}}} \sum_{j=1}^{N_{\mathcal{T}}} H(q_{\Theta_{E,i}}(s_i^{(j)} | z_i^{(j)}), \varepsilon_{s_i}^{(j)}), \quad i \in [M] \quad (8)$$

Note that all the adversarial networks can be trained in parallel. The distortion measure we consider for our legitimate loss function \mathcal{L}_{AB} is a mixture of the average MSE, denoted by Δ^{MSE} , and SSIM, Δ^{SSIM} , between the input image \mathbf{u} and the recovered pixels $\hat{\mathbf{u}}$ at the output of Bobs' DNN. Therefore, we assume $d(\cdot, \cdot)$ to be measured as follows

$$d(\mathbf{u}, \hat{\mathbf{u}}) = \Delta^{\text{MSE}} + \alpha \Delta^{\text{SSIM}}, \quad (9)$$

where

$$\Delta^{\text{MSE}} = \frac{1}{n} \|\mathbf{u} - \hat{\mathbf{u}}\|^2, \quad \Delta^{\text{SSIM}} = 1 - \text{SSIM}(\mathbf{u}, \hat{\mathbf{u}}), \quad (10)$$

with n denoting the size of the original image vector $\mathbf{u} \in \mathbb{R}^n$. Moreover, α is a tuning parameter representing the contribution of SSIM metric in the distortion measure $d(\cdot, \cdot)$. The SSIM measure between two images I and K is defined as

$$\text{SSIM}(I, K) \triangleq \frac{(2\mu_I \mu_K + c_1)(2\sigma_{IK} + c_2)}{(\mu_I^2 + \mu_K^2 + c_1)(\sigma_I^2 + \sigma_K^2 + c_2)}, \quad (11)$$

where $\mu_I, \mu_K, \sigma_I, \sigma_K$, and σ_{IK} are the local means, standard deviations, and cross-covariance for images I and K . c_1 and c_2 are two adjustable constants [33]. We note that the SSIM index is a *perception-based metric*, which is able to capture pixel inter-dependencies even for spatially close pixels. The rationale behind assuming the proposed distortion metric in (9) is that we not only aim to recover every pixel of a source image with minimum error (realized via MSE measure), but also want to obtain a good-quality reconstruction from the human visual system point of view. We also remark that SSIM calculation is relatively simple, and its derivatives can be easily computed within the gradient descent-based algorithms [34]. In addition, it is shown in [33] that leveraging perceptual-based metrics to reconstruct images can lead to better results in content-aware learning tasks. The training procedure can be carried out efficiently, using off-the-shelf stochastic gradient descent algorithms with fast convergence. We have chosen the widely-adopted adaptive moment estimation (Adam) optimizer algorithm [38] for minimizing (7) and (8). More details are provided in the next section.

TABLE I: Parameters for Training the Proposed System

Learning Parameters	Values
Batch size (m)	128
Maximum number of training episodes (N_{episode})	200
Number of warm-up epochs ($N_{\text{warm-up}}$)	50
Number of legitimate training epochs per episode (N_L)	5
Number of adversarial training epochs per episode (N_E)	5
Training SNR of legitimate link (Γ_L^{train})	20
Training SNR of adversarial links (Γ_E^{train})	15
Learning rate	10^{-4}

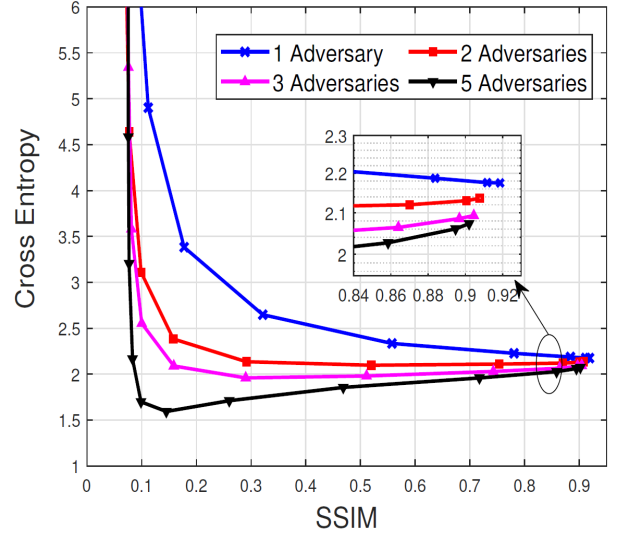


Fig. 4: Privacy-utility trade-off over CIFAR-10.

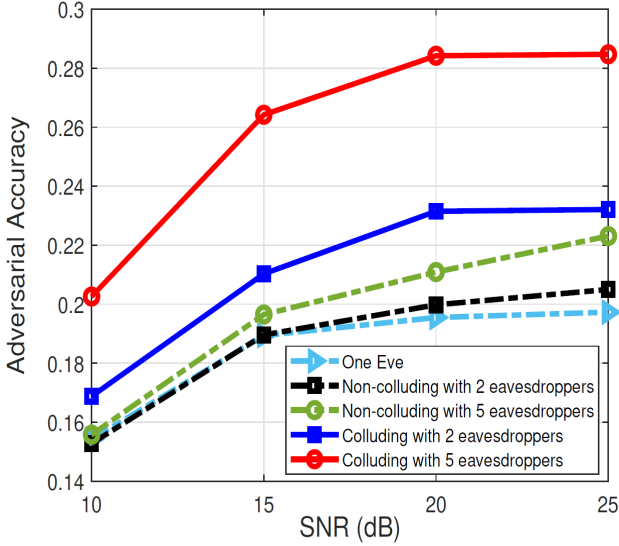
IV. IMPLEMENTATION AND EVALUATION

In this section, we present different experiments to demonstrate the performance of our proposed deep learning-based approach in various scenarios. Different benchmarks and ablation studies are also provided to show the efficiency of our proposed scheme. We consider both scenarios of colluding and non-colluding eavesdroppers. In addition, we study both cases of eavesdroppers being interested in a common secret S , and the case in which every eavesdropper is interested in a different secret, using two different datasets of CIFAR-10 [36] and CelebA [37], respectively. We examine the performance over both AWGN and complex fading (Rayleigh and Nakagami- m) communication channels for different channel SNRs and $n_{\mathcal{T}} = 4$ antennas (unless otherwise stated). Moreover, we address the generalization capability of our proposed scheme for different communication scenarios and over a wide range of channel SNRs, to highlight the *robustness* and *data efficiency* of our proposed learning-based secrecy-preserving solution. We also study the *privacy-utility trade-off* for the proposed learning-based approach, which provides useful insights on the concept of secure communications.

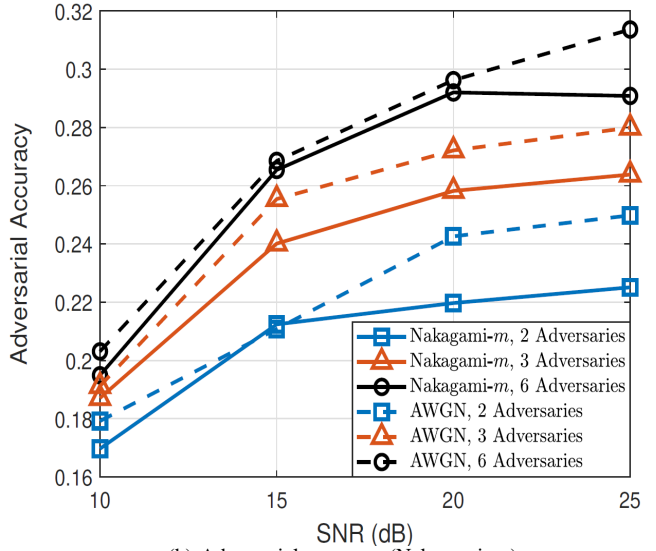
The SNRs of communication links are defined as:

$$\Gamma_L = 10 \log_{10} \frac{P}{\sigma_L^2} \quad (\text{dB}), \quad \Gamma_E = 10 \log_{10} \frac{P}{\sigma_E^2} \quad (\text{dB}), \quad (12)$$

which represent the ratio of the average power of the encoded data-stream of the latent space (i.e., the channel input) to the average noise power of legitimate σ_L^2 and adversarial



(a) Adversarial accuracy (Rayleigh)

(b) Adversarial accuracy (Nakagami- m)Fig. 5: Adversarial accuracy vs. SNR (Γ_E) for Rayleigh fading, AWGN, and Nakagami- m (with $m = 3$) channels.

nodes σ_E^2 , respectively. Without loss of generality, we set the average signal power to $P = 1$ for all experiments, while varying the SNR by setting the noise variances σ_L^2 and σ_E^2 . The std of the eavesdropping channels are set to $\{0.04, 0.16, 0.36, 0.64, 1, 1.44\}$ for $i \in [6]$, for $M = 6$ simulated eavesdroppers in total. The bandwidth compression ratio is set to $\frac{k}{n} = \frac{1}{3}$. For simplicity, we consider a single weight in the loss function, that is, $w_i = w, \forall i$. We set $w = 5$ and $\alpha = 0.1$ during training, which is elaborated in the subsequent numerical experiments. For the training, we have assumed the general case of complex Rayleigh fading channel model which is treated by the joint effect of channel fading and additive noise, i.e., $\eta(\tau) = \eta_\nu(\eta_h(\tau)) = h\tau + \nu$ with $h \sim \mathcal{CN}(0, 1)$. Nevertheless, during the inference phase we study the performance of our proposed scheme in different scenarios of AWGN and Nakagami- m channels $|h|^2 \sim \mathcal{G}(m, \delta_h^2/m)$.

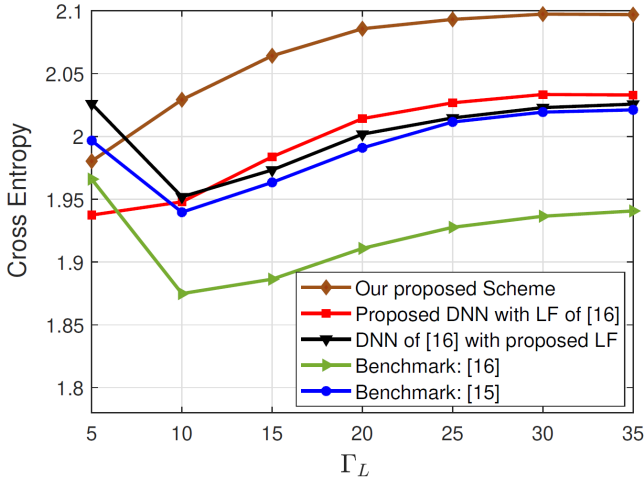
We have implemented our proposed network architecture (shown in Figs. 2 and 3) using Python3 with Tensorflow [35]. The codes were run on Intel(R) Xeon(R) Silver 4114 CPU running at 2.20 GHz with GeForce RTX 2080 Ti GPU. To minimize the legitimate and adversarial loss functions (LFs), we have chosen the widely-adopted Adam optimizer algorithm [38]. Similarly to [16], we choose to fix the number of training episodes N_{episode} in advance, where the value of $N_{\text{episode}} = 200$ is set according to our experiments. The learning parameters used during the training process are summarized in Table I. The detailed description of training process can be stated as follows. i) During a *warm-up phase*, both legitimate pairs and adversarial networks are independently trained in order to reach a plausible initial state of reconstructing the image. To elaborate, for $N_{\text{warm-up}} = 50$ epochs, the encoder-decoder pair of Alice and Bob (Ω_A, Ω_B) are trained according to the reconstruction objective of minimizing $\mathcal{L}_{AB}^{\text{warm-up}} = \frac{1}{N_T} \sum_{i=1}^{N_T} d(\mathbf{u}_i, \hat{\mathbf{u}}_i)$, where $d(\cdot, \cdot)$ is given in (9). Following the legitimate warm-up, the adversarial networks ($\Theta_{E,1}, \dots, \Theta_{E,M}$) are trained for $N_{\text{warm-up}} = 50$ epochs,

while the legitimate encoder Ω_A is frozen. ii) After performing the warm-up, the main phase of *minimax training* starts. In this phase, for each of the $N_{\text{episode}} = 200$ episodes, Alice and Bob aim to learn the optimal mapping for the latent space and the decoding neural structure so that the reconstruction distortion and information leakage are minimized. Hence, the legitimate encoder-decoder counterparts (Ω_A, Ω_B) are trained for $N_L = 5$ epochs based on minimizing the LF $\mathcal{L}_{AB}^{\text{ALC}}$ given in (7). Since the neural encoder Ω_A at Alice has learned a new embedding for the original data, the adversaries are then trained for $N_E = 5$ epochs to learn and adjust their adversarial role in extracting sensitive information from the newly-learned latent space based on the LF, \mathcal{L}_E , given in (8). In this manner, the concept of minimax game between $(\mathcal{A}, \mathcal{B})$ and the set of eavesdroppers is realized, while maintaining the fairness for the learning process of legitimate and adversarial nodes.

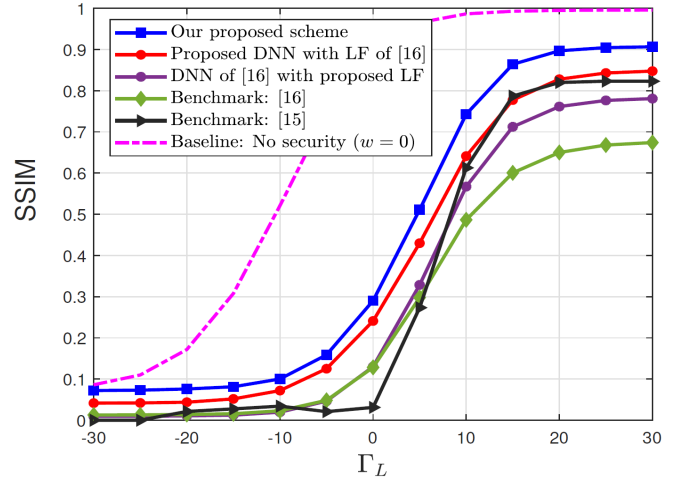
A. Evaluation on CIFAR-10 dataset

We evaluate our proposed secure framework using images with dimension $32 \times 32 \times 3$ (height, width, channels) from the CIFAR-10 dataset [36]. The dataset consists of 60000 colored images of size 32×32 pixels. The training and evaluation sets are two completely separated sets of images, containing 50000 and 10000 images, respectively, associated with 10 classes. Adversaries wish to infer a common secret S from the noisy encoded signals through their own channels, either individually (i.e., the non-colluding case), or by learning from the combination of the individual logits extracted by adversaries (i.e., the colluding setup). Hence, the common secret S here is considered as the class of CIFAR-10 images with $|S| = L = 10$.

In the following experiments, we evaluate the performance of our proposed scheme during the inference phase. We also highlight that our proposed approach is *generalizable* and performs well in different types of communication channels and eavesdropping scenarios.



(a) Ablation study in terms of CE



(b) Ablation study in terms of SSIM

Fig. 6: Ablation studies in terms of CE and SSIM metrics during inference.

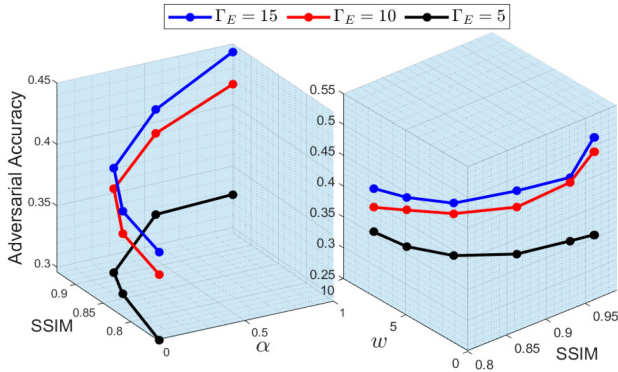
Fig. 7: Effect of α and w on the privacy-utility trade-off

Fig. 4 demonstrates the *privacy-utility trade-off* for our proposed secure framework. The figure is obtained for the legitimate SNR from $\Gamma_L = -20$ dB to 30 dB with steps of 5 dB. The figure addresses the fact that by improving the quality of the reconstructed image in SSIM, it is inevitable to have a certain level of information leakage (measured via the CE) in general. This phenomena, which is actually in accordance with one’s intuition, also verifies our generic mathematical framework proposed in (1). The point of this figure is that by increasing the SNR and gradually improving the quality of data reconstruction (increasing the SSIM at Bob), the value of CE soon saturates. After that, we can achieve higher SSIMs without any significant increase in the leakage. For instance, for the case of having $M = 3$ adversaries, by setting $\Gamma_L \geq 5$ dB, we can enhance the image reconstruction at Bob’s decoder, without any further decrease in CE values. In this case, 15 dB increase in channel SNR can improve the SSIM about 56%. Therefore, such trade-off curves can help network designers adjust the system parameters to achieve desired levels of secrecy and utility. The figure also indicates that having more adversaries results in more leakage (less CE). The (small) negative impact of adversaries on the SSIM values can be explained by the minimax game invoked by (2) and

proposed in Sections III-C and IV, which mutually affects the performance of legitimate counterparts as well.

Figs. 5-(a) and 5-(b) demonstrate the adversarial accuracy of our proposed scheme for the scenario of colluding eavesdroppers. For this experiment, we study the performance of *colluding adversarial inference*, and compare it with the non-colluding setup. We note that for the non-colluding setup, the training is performed based on (7)–(9), and the eavesdroppers try to extract the common or individual secret S_i based on their own loss functions given in (8). Meanwhile, for the colluding setup (with a common secret S) an extra level of “knowledge combination” is performed afterward—we combine the individually-extracted logits of adversaries, and leverage the concept of *ensemble learning* to infer the secret S . For the colluding setup, the adversarial performance is measured by the overall accuracy of adversaries in correctly finding the ground-truth ε_s from their aggregated logits, while for the non-colluding benchmarks, the mean accuracy across eavesdroppers is plotted for the sake of comparison. The overall accuracy of adversaries is plotted versus channel SNR of the wiretap links, Γ_E , for different number of eavesdroppers and different types of communication channels. We can observe from the figures that increasing the number of eavesdroppers results in achieving higher accuracy for the adversaries, which is aligned with one’s intuition. The increase in adversarial accuracy is more significant in the colluding case, due to the collaboration and knowledge combination among eavesdroppers which helps them learn the secret more accurately. Figs. 5-(a) and 5-(b) indicate that by increasing the quality of adversarial links, i.e., increasing Γ_E , the accuracy of adversaries increases by at most 10%. This can be observed from (12), where higher values for Γ_E results in having less-distorted (less noisy) observations $Z_i^k = z_i$, $i \in [M]$, at the adversarial DNNs, which results in more accurate estimations about the posterior adversarial distribution $q_{\Theta_{E,i}}(s|z_i)$, with respect to the ground-truth ε_s . Interestingly, the amount of increase in the adversarial accuracy reduces with the increase in Γ_E , which highlights the limitation of adversarial nodes

based on our proposed secure scheme. Fig. 5-(b) also addresses the generalization capability of our learning-based framework extended to the AWGN communication model and Nakagami- m scenario $|h|^2 \sim \mathcal{G}(m, 1/m)$. This experiment verifies that we can achieve almost similar performance in other channel scenarios, despite being trained for the Rayleigh fading case, which highlights the *robustness* and *generalizability* of our proposed scheme.

Fig. 6-(a) demonstrates the CE metric for our proposed scheme compared with different benchmarks. Notably, this figure highlights the superiority of our approach compared to the benchmarks of [16] and [15]. This figure also implies that increasing the SNR of legitimate link Γ_L results in having higher CE values, thus lower information leakage can be achieved in terms of lower similarity between the posterior adversarial likelihood and the ground-truth. This is because increasing Γ_L (given in (12)) results in less noisy observations at Bob than the adversarial DNNs. Therefore, Alice can better hide the sensitive attributes in noise, making it harder for the adversaries to extract the sensitive information from distorted received data.

Fig. 6-(b) illustrates the data reconstruction performance of our proposed framework compared with other benchmarks. One can infer from this figure and Fig. 6-(a) that our proposed system outperforms the benchmarks in terms of both secrecy and utility. Accordingly, 20% and 10% performance gain is achieved by our proposed scheme compared with [16] and [15], respectively. Fig. 6-(b) also implies that increasing Γ_L results in having higher SSIM values. This is because increasing Γ_L results in less distorted observations at Bob, which facilitates the image reconstruction performance of Bob's neural decoder. Notably, Fig. 6-(b) highlights that if we neglect the existence of adversaries and set $w = 0$, our proposed scheme can achieve almost perfect (SSIM = 1) data recovery. The ablation-like examinations conducted in Figs. 6-(a) and 6-(b) imply that both the DNN structure and the employed LF for optimizing the framework contribute to the overall secrecy and reconstruction performance. Specifically, our proposed DNNs at Alice and Bob, together with the proposed objective function elaborated in (5) and (7)–(9) have resulted in achieving the best performance compared with other benchmarks and baselines.

Remark 3: Figs. 6-(a) and 6-(b) validate the *data efficiency* and *generalizability* of our proposed scheme, since we have trained our DNNs with a fixed SNR $\Gamma_L^{\text{train}} = 20$, while the performance gain of our approach during inference holds for a wide range of SNRs.

Fig. 7 studies the impact of tuning parameters α and w on the adversarial performance of our proposed system. These tuning parameters are the coefficients associated with utility and secrecy adjustment terms within our training LF in (9) and (7), respectively. For this experiment, the adversarial performance is captured by investigating the accuracy of adversaries in correctly finding the ground-truth label ε_s (representing the sensitive information S) out of $L = 10$ labels of CIFAR-10 dataset. For the accuracy measurement in this experiment, we consider the pessimistic scenario in which the correct guess of true labels by any adversary $i \in [M]$ increments

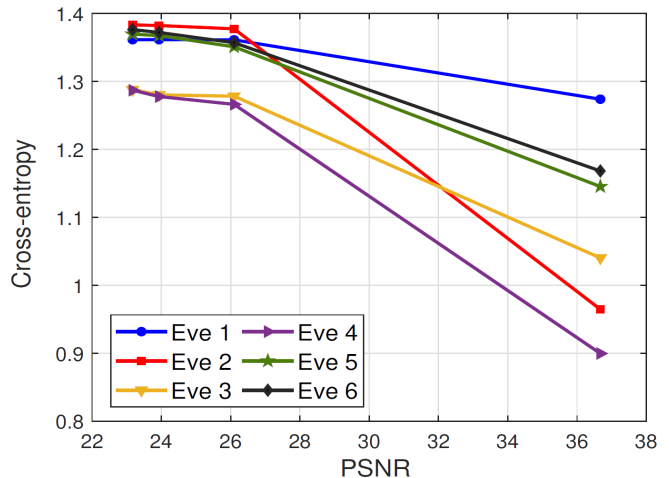


Fig. 8: Privacy-utility trade-off over CelebA dataset.

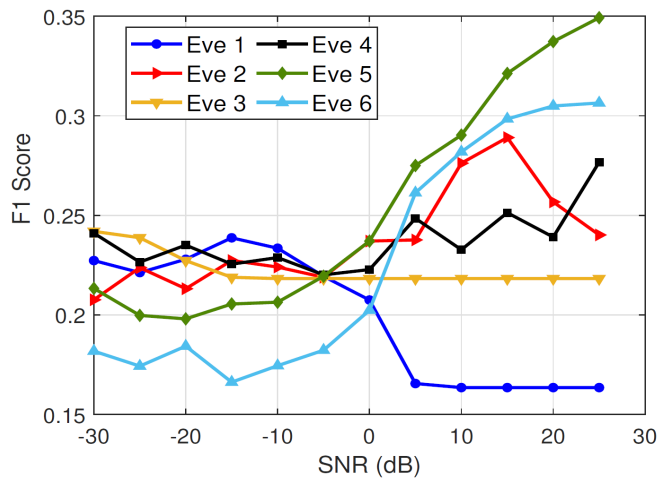


Fig. 9: Adversarial accuracy in terms of F1 score over CelebA dataset.

the total accuracy of adversaries. The figure indicates that by increasing α , higher values of SSIM can be achieved, since more emphasis on the SSIM error Δ^{SSIM} is put based on (9). However, the accuracy of adversaries in extracting the private information also increases, which verifies the privacy-utility trade-off. Notably, by increasing α to values more than 0.1, a jump in the adversarial accuracy can be observed, which lead us choosing $\alpha = 0.1$ for our network. Similarly, by increasing w , the emphasis goes toward the secrecy criteria introduced in (1), (5), and (7), which leads to the reduction in adversarial accuracy and achieved SSIM, verifying the privacy-utility trade-off as well. The figure also shows that increasing the adversary channels SNR Γ_E can improve the adversarial accuracy in finding the sensitive data ε_s . Interestingly, the amount of increase in the adversarial accuracy reduces with the increase in Γ_E which highlights the limitation of adversarial nodes based on our proposed secure scheme.

B. Evaluation on CelebA dataset

In this subsection, we evaluate our proposed scheme on CelebA dataset [37]. This is a large-scale face attributes dataset with more than 200k images of celebrities with 40 attribute

TABLE II: Privatized CelebA Attributes for Each Eavesdropper

Eavesdropper	Private Attributes
Eve 1	Wavy_Hair and Black_Hair
Eve 2	Wearing_Lipstick and Smiling
Eve 3	Double_Chin and Wearing_Necklace
Eve 4	No_Beard and 5_o_Clock_Shadow
Eve 5	Bags_Under_Eyes and Arched_Eyebrows
Eve 6	High_Cheekbones and Pointy_Nose

annotations. For the following experiments, we consider the non-colluding scenario, in which eavesdroppers are interested in *different secrets* $S_i \in \mathcal{S}_i$, while we assume $|S_i| = 4$ for all eavesdroppers. Details of the privatized attributes for each eavesdropper $i \in [M]$ are provided in Table II.

Fig. 8 demonstrates the privacy-utility trade-off over CelebA dataset with SNR $\Gamma_E = 25$ dB. Since the eavesdroppers are interested in different secrets, the results are plotted for each individual eavesdropper $i \in [6]$. The figure is obtained by changing the hyperparameter $w \in \{0, 10, 50, 100\}$, which shapes the secrecy funnel within our framework in (5). In this figure, the extreme case of $w = 100$ has the minimum leakage, i.e., the maximum CE, $H(q_{\Theta_{E,i}}(s_i|z_i), \epsilon_{s_i})$, while having the minimum utility (reflected by the PSNR metric in this experiment). This is because larger w implies that DNN encoder-decoder pair gives more importance to the secrecy criteria in (5)–(7). However, as we gradually decrease w , higher PSNRs can be achieved with a slight increase in the information leakage. The figure also implies that for the baseline of no security design, i.e., $w = 0$, the information leakage increases by about 30%, which highlights the importance of designing a secure neural encoding-decoding pair.

Fig. 9 shows the accuracy of eavesdroppers versus Γ_E for $w = 10$. Since the CelebA is a highly *imbalanced dataset* with respect to most of the attributes, we have chosen the F-score metric with macro averaging to measure the adversarial accuracy in this scenario. Note that due to the imbalance in CelebA dataset attributes, we employed a penalty mechanism. However, we still observe the effect of the imbalance on the eavesdroppers in terms of F-scores. The figure indicates that our implemented secure neural encoding-decoding pair has been successful in confusing Eves about the private attributes, as a maximum of 25% accuracy is achieved by adversaries for most of the SNR values. Similar to the results over CIFAR-10, this figure also indicates that increasing the quality of adversarial links can increase the accuracy of eavesdroppers by at most 15%.

Fig. 10 illustrates the reconstruction quality (for different values of w) at Bob and each of the eavesdroppers. We can observe that the bigger w , the worse would be the reconstruction quality at Eves (and also at Bob), as the emphasis shifts toward the secrecy criteria. The figure also implies that the eavesdroppers are strongly restrained from reconstructing any meaningful (high perceptual quality) images, due to very low adversarial SSIM values.

To gain visual insights into the reconstruction performance of Bob, and what the reconstructed images at eavesdroppers would be like, Fig. 11 is provided. Please note that the goal of eavesdroppers is to infer the secrets rather than reconstruct the entire image. We show the reconstructions at

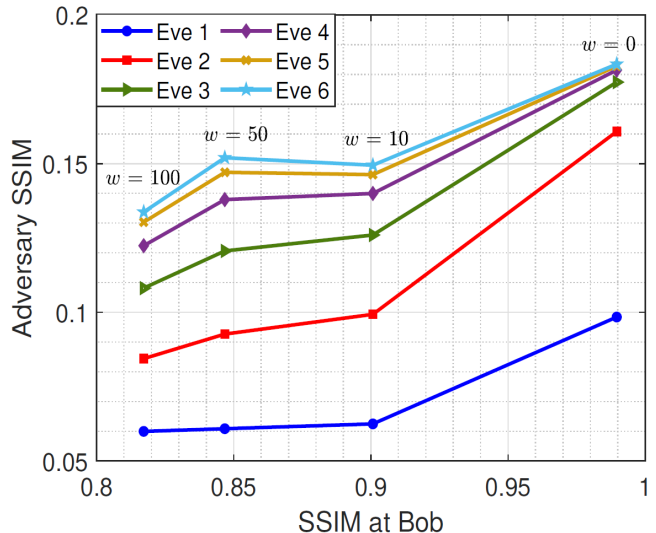


Fig. 10: Reconstruction quality of the legitimate destination vs. the eavesdroppers over CelebA dataset.

the eavesdroppers only for illustration purposes. To this end, the legitimate DNN encoder is frozen after being trained for 180 epochs, and then, a similar neural structure to that of Bob is considered for each of the eavesdroppers, which gets trained for image reconstruction.⁵ The reconstructed images in Fig. 11 correspond to the default case of $w = 10$, and the extreme case of $w = 100$. Interestingly, one can observe that our proposed secure framework has been successful in hiding the corresponding private information against each eavesdropper, e.g., the hair style, smiling, facial attributes, etc., while recovering the entire image at Bob such that it can be distinguished clearly. Notably, although the main objective of the legitimate encoder was to prevent adversaries from extracting the “privatized data,” we can also observe that the eavesdroppers cannot successfully reconstruct the images either.

V. CONCLUSIONS

In this paper, we proposed a DeepJSCC approach for E2E secure image delivery against multiple eavesdroppers over AWGN as well as complex-valued fading channels. We considered both scenarios of colluding and non-colluding eavesdroppers over CIFAR-10 and CelebA datasets. The adversarial DNNs try to extract the sensitive information from the noisy channel outputs they observe, while the legitimate pair of Alice and Bob wish to have a secure communication with minimum average distortion, leading to a minimax game between Alice-Bob pair and the eavesdroppers. We introduced a context-aware and data-driven approach to realize E2E secure transmission through learning from available datasets. We leveraged the concept of autoencoders and proposed our neural encoder-decoder pair together with a secrecy funnel framework to achieve both secrecy and utility, where we also take into account the perceptual quality of image transmission within our DNNs and LF. Extensive ablation studies and

⁵During the evaluation, we transmit each image 10 times and the performance metrics are averaged over these realizations.

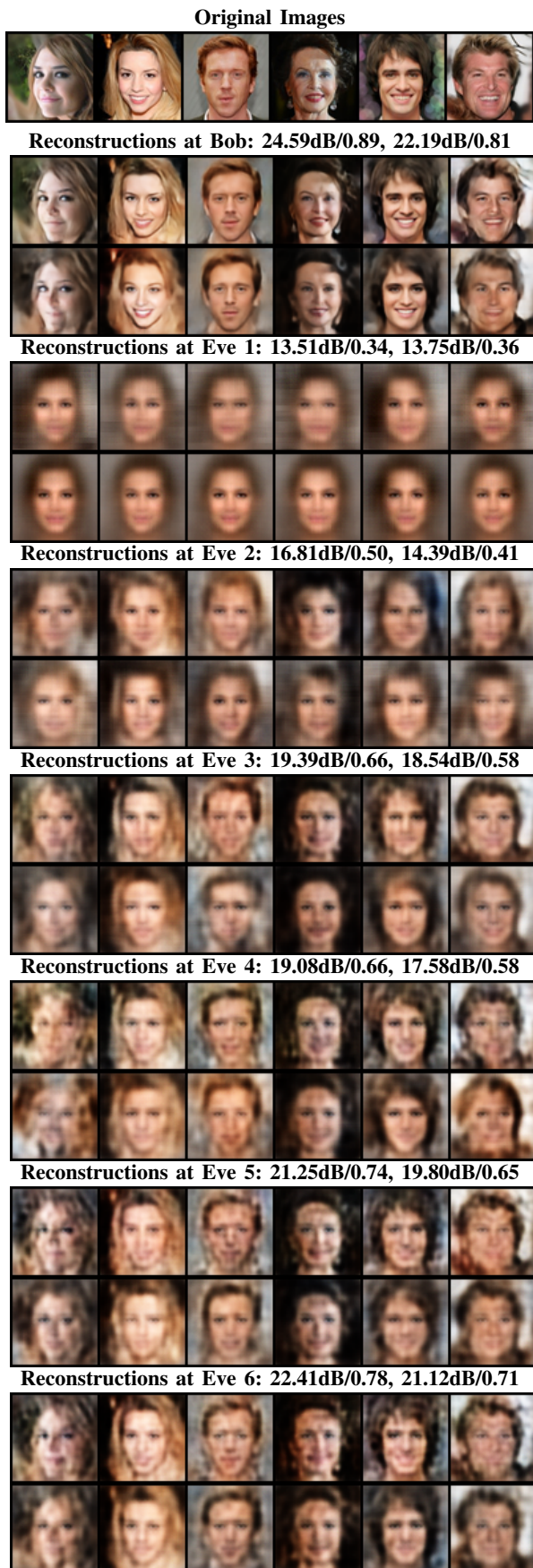


Fig. 11: Reconstructed CelebA images at Bob and each Eve. For each set of images, the first and second rows correspond to $w=10$ and $w=100$, respectively. PSNR(dB)/SSIM values are provided above each set of images.

visual tests validate the performance gain of our proposed scheme compared with related benchmarks, while addressing the privacy-utility trade-off. Our proposed system is also shown to be *generalizable* to a wide range of SNRs and different communication scenarios.

REFERENCES

- [1] S. A. Ameli Kalkhoran, M. Letafati, E. Erdemir, B. H. Khalaj, H. Behroozi and D. Gündüz, "Secure deep-JSCC against multiple eavesdroppers," *2023 IEEE Global Communications Conference (GLOBECOM 2023)*, Kuala Lumpur, Malaysia, Dec. 2023, pp. 3433-3438.
- [2] H. Li, K. Ota and M. Dong, "Learning IoV in 6G: Intelligent edge computing for Internet of Vehicles in 6G wireless communications," *IEEE Wireless Communications*, vol. 30, no. 6, pp. 96-101, Dec. 2023.
- [3] F. Hu, Y. Deng, W. Saad, M. Bennis, and A. H. Aghvami, "Cellular-connected wireless virtual reality: Requirements, challenges, and solutions," *IEEE Comm. Mag.*, vol. 58, no. 5, pp. 105-111, May 2020.
- [4] M. Jankowski, D. Gündüz, and K. Mikołajczyk, "Wireless image retrieval at the edge," *IEEE J. Sel. Areas Comm.*, vol. 39, no. 1, pp. 89-100, Jan. 2021.
- [5] M. Letafati, H. Behroozi, B. H. Khalaj, and E. A. Jorswieck, "Deep learning for hardware-impaired wireless secret key generation with man-in-the-middle attacks," *2021 IEEE Global Communications Conference (GLOBECOM)*, Madrid, Spain, Dec. 2021, pp. 1-6.
- [6] —, "Learning-based secret key generation in relay channels under adversarial attacks," *IEEE Open Journal of Vehicular Technology*, vol. 4, pp. 749-764, Sep. 2023.
- [7] M. Letafati, A. Kuhestani, H. Behroozi and D. W. K. Ng, "Jamming-resilient frequency hopping-aided secure communication for Internet-of-Things in the presence of an untrusted relay," *IEEE Trans. on Wireless Comm.*, vol. 19, no. 10, pp. 6771-6785, Oct. 2020.
- [8] M. Letafati, H. Behroozi, B. H. Khalaj, and E. A. Jorswieck, "Hardware-impaired PHY secret key generation with man-in-the-middle adversaries," *IEEE Wireless Comm. Lett.*, vol. 11, no. 4, pp. 856-860, Apr. 2022.
- [9] —, "Wireless-powered cooperative key generation for e-health: A reservoir learning approach," *2022 IEEE 95th Vehicular Technology Conference (VTC-Spring)*, Helsinki, Finland, Jun. 2022, pp. 1-7.
- [10] M. Letafati, A. Kuhestani, K. -K. Wong and M. J. Piran, "A lightweight secure and resilient transmission scheme for the Internet-of-Things in the presence of a hostile jammer," *IEEE Internet of Things J.*, Sep. 2020.
- [11] A. Chorti, A. N. Barreto, S. Kopsell, M. Zoli, M. Chaffi, P. Sehier, G. Fettweis, and H. V. Poor, "Context-aware security for 6G wireless: The role of physical layer security," *IEEE Communications Standards Magazine*, vol. 6, no. 1, pp. 102-108, Mar. 2022.
- [12] M. Letafati, H. Behroozi, B. H. Khalaj, and E. A. Jorswieck, "On learning-assisted content-based secure image transmission for delay-aware systems with randomly-distributed eavesdroppers," *IEEE Trans. Comm.*, vol. 70, no. 2, pp. 1125-1139, Feb. 2022.
- [13] —, "Content-based medical image transmission against randomly-distributed passive eavesdroppers," *IEEE Int. Conf. Comm. Workshop (ICCW)*, Montreal, Canada, Jun. 2021, pp. 1-7.
- [14] E. Bourtsoulatzé, D. Burth Kurka, and D. Gündüz, "Deep joint source-channel coding for wireless image transmission," *IEEE Trans. Cogn. Comm. Netw.*, vol. 5, no. 3, pp. 567-579, Sep. 2019.
- [15] D. B. Kurka and D. Gündüz, "DeepJSCC-f: Deep joint source-channel coding of images with feedback," *IEEE Journal on Selected Areas in Information Theory*, vol. 1, no. 1, pp. 178-193, May 2020.
- [16] T. Marchioro, N. Laurenti, and D. Gündüz, "Adversarial networks for secure wireless communications," *2020 IEEE Int. Conf. Acoust. Speech Signal Process (ICASSP)*, Barcelona, Spain, May 2020, pp. 8748-8752.
- [17] E. Erdemir, P. L. Dragotti and D. Gündüz, "Privacy-aware communication over a wiretap channel with generative networks," *IEEE Int. Conf. Acoust. Speech Signal Process. (ICASSP)*, Marina Bay Sands, Singapore, May 2022, pp. 2989-2993.
- [18] K. -L. Besser, C. R. Janda, P. -H. Lin, and E. A. Jorswieck, "Flexible design of finite blocklength wiretap codes by autoencoders," in *Proc. IEEE Int. Conf. Acoust., Speech, Sig. Proc.*, pp. 2512-2516, May 2019.
- [19] K. -L. Besser, P. -H. Lin, C. R. Janda, and E. A. Jorswieck, "Wiretap code design by neural network autoencoders," *IEEE Trans. Inf. Forensics Secur.*, vol. 15, pp. 3374-3386, Oct. 2019.
- [20] R. Fritschek, R. F. Schaefer, and G. Wunder, "Deep learning based wiretap coding via mutual information estimation," in *Proceedings of the 2nd ACM Workshop on Wireless Security and Machine Learning (WiseML'20)*, NY, USA, Jul. 2020, pp. 74-79.

- [21] T. -Y. Tung and D. Gündüz, "Deep joint source-channel and encryption coding: Secure semantic communications," *2023 IEEE International Conference on Communications (ICC)*, Rome, Italy, May 2023, pp. 5620–5625.
- [22] J. Xu, B. Ai, W. Chen, N. Wang and M. Rodrigues, "Deep joint source-channel coding for image transmission with visual protection," *IEEE Transactions on Cognitive Communications and Networking*, vol. 9, no. 6, pp. 1399-1411, Dec. 2023.
- [23] M. Zhang, Y. Li, Z. Zhang, G. Zhu and C. Zhong, "Wireless image transmission with semantic and security awareness," *IEEE Wireless Communications Letters*, vol. 12, no. 8, pp. 1389–1393, Aug. 2023.
- [24] S. Tang, C. Liu, Q. Yang, S. He, and D. Niyato, "Secure semantic communication for image transmission in the presence of eavesdroppers," *arXiv preprint arXiv:2404.12170*, Apr. 2024.
- [25] Y. E. Sagduyu, T. Erpek, S. Ulukus and A. Yener, "Is semantic communication secure? A tale of multi-domain adversarial attacks," *IEEE Communications Magazine*, vol. 61, no. 11, pp. 50–55, Nov. 2023.
- [26] J. Ballé, V. Laparra, and E. P. Simoncelli, "Density modeling of images using a generalized normalization transformation," in *4th International Conference on Learning Representations (ICLR 2016)*, 2016.
- [27] N. Merhav, "On joint coding for watermarking and encryption," *IEEE Trans. Info. Theory*, vol. 52, no. 1, pp. 190-205, Jan. 2006.
- [28] A. Makhdoumi, S. Salamatian, N. Fawaz, and M. Médard, "From the information bottleneck to the privacy funnel," in *Proc. of IEEE Information Theory Workshop (ITW)*, 2014.
- [29] E. Björnson, E. A. Jorswieck, M. Debbah, and B. Ottersten, "Multiobjective Signal Processing Optimization: The way to balance conflicting metrics in 5G systems," *IEEE Signal Processing Magazine*, vol. 31, no. 6, pp. 14–23, Nov. 2014.
- [30] D. Barber and F. Agakov, "The IM algorithm: A variational approach to information maximization," *Advances in Neural Information Processing Systems 16: Proceedings of the 2003 Conference*, vol. 16, pp. 201–208.
- [31] K. He, X. Zhang, S. Ren, and J. Sun, "Delving deep into rectifiers: Surpassing human-level performance on imagenet classification," *IEEE Int'l Conf. Comput. Vision (ICCV)*, pp. 1026–1034, Dec. 2015.
- [32] J. L. Ba, J. R. Kiros, and G. E. Hinton, "Layer normalization," 2016, *arXiv:1607.06450*. [Online]. Available: <https://arxiv.org/abs/1607.06450>.
- [33] J. Snell, K. Ridgeway, R. Liao, B. D. Roads, M. C. Mozer, and R. S. Zemel, "Learning to generate images with perceptual similarity metrics," *2017 IEEE International Conference on Image Processing (ICIP)*, pp. 4277–4281, Sep. 2017.
- [34] H. Zhao, O. Gallo, I. Frosio, and J. Kautz, "Loss functions for image restoration with neural networks," *IEEE Transactions on Computational Imaging*, vol. 3, pp. 47–57, Mar. 2017.
- [35] M. Abadi *et al.*, "TensorFlow: Large-scale machine learning on heterogeneous systems," software available from tensorflow.org. [Online]. Available: <https://www.tensorflow.org/>
- [36] A. Krizhevsky, "Learning multiple layers of features from tiny images," University of Toronto, Tech. Rep., 2009.
- [37] Liu, Z., Luo, P., Wang, X., Tang, X., "Deep learning face attributes in the wild," in *Proc. Int'l Conf. on Computer Vision (ICCV)*, Dec. 2015.
- [38] D.P. Kingma and L.J. Ba, "Adam: A method for stochastic optimization," *2015 International Conference on Learning Representations (ICLR)*, San Diego, May 2015, pp. 1–13.